ARTICLE
Journal of Cellular Biochemistry 113:3313–3329 (2012)

Journal of Cellular Biochemistry

Arrangement of Nuclear Structures Is Not Transmitted Through Mitosis But Is Identical in Sister Cells

Darya Yu. Orlova,[1,2] Lenka Stixová,[1] Stanislav Kozubek,[1] Hinco J. Gierman,[3] Gabriela Šustáčková,[1] Andrei V. Chernyshev,[2] Ruslan N. Medvedev,[2] Soňa Legartová,[1] Rogier Versteeg,[4] Pavel Matula,[1,5] Roman Stoklasa,[5] and Eva Bártová[1*]

[1]*Institute of Biophysics, Academy of Sciences of the Czech Republic, v.v.i., Královopolská 135, CZ-612 65 Brno, Czech Republic*

[2]*Institute of Chemical Kinetics and Combustion, Institutskaya 3, 630090 Novosibirsk, Russia*

[3]*Department of Developmental Biology, Stanford University, 279 Campus Drive, Stanford, California 94305*

[4]*Department of Oncogenomics, Amsterdam Medical Center, University of Amsterdam, Amsterdam, The Netherlands*

[5]*Faculty of Informatics, Masaryk University, Botanická 68a, 602 00 Brno, Czech Republic*

ABSTRACT

Although it is well known that chromosomes are non-randomly organized during interphase, it is not completely clear whether higher-order chromatin structure is transmitted from mother to daughter cells. Therefore, we addressed the question of how chromatin is rearranged during interphase and whether heterochromatin pattern is transmitted after mitosis. We additionally tested the similarity of chromatin arrangement in sister interphase nuclei. We noticed a very active cell rotation during interphase, especially when histone hyperacetylation was induced or transcription was inhibited. This natural phenomenon can influence the analysis of nuclear arrangement. Using photoconversion of Dendra2-tagged core histone H4 we showed that the distribution of chromatin in daughter interphase nuclei differed from that in mother cells. Similarly, the nuclear distribution of heterochromatin protein 1β (HP1β) was not completely identical in mother and daughter cells. However, identity between mother and daughter cells was in many cases evidenced by nucleolar composition. Moreover, morphology of nucleoli, HP1β protein, Cajal bodies, chromosome territories, and gene transcripts were identical in sister cell nuclei. We conclude that the arrangement of interphase chromatin is not transmitted through mitosis, but the nuclear pattern is identical in naturally synchronized sister cells. It is also necessary to take into account the possibility that cell rotation and the degree of chromatin condensation during functionally specific cell cycle phases might influence our view of nuclear architecture. J. Cell. Biochem. 113: 3313–3329, 2012.

KEY WORDS: HISTONES; CHROMATIN; HP1 PROTEIN; PHOTOCONVERSION; DENDRA2; CAJAL BODIES

Chromosomes are very prominent nuclear structures that exhibit varying degrees of compaction during the cell cycle. Moreover, pronounced chromosome condensation can occur during cell differentiation or may accompany apoptotic processes. The existence of compact chromosomes in interphase nuclei of animal cells was originally suggested by Rabl [1885] and was confirmed by Boveri [1909]. Boveri studied horse parasitic nematodes, characterized by either one or two pairs of germline chromosomes. Using simple experimental approaches, he came to the conclusion that individual chromosomes, visible in metaphase, could maintain their specific shape within interphase. Later, with the development of more advanced techniques, it was confirmed that particular interphase chromosomes occupy specific nuclear regions called chromosome territories (CTs) [summarized by Cremer and Cremer,

Abbreviations used: HP1, heterochromatin protein 1; WLL, white light laser; RIDGEs, regions of increased gene expression; anti-RIDGE regions, regions of low gene expression; TSA, trichostatin A; FISH, fluorescence in situ hybridization; UV, ultraviolet.

The authors indicate no potential conflict of interest.

Additional supporting information may be found in the online version of this article.

Grant sponsor: Grant Agency of Czech Republic; Grant numbers: P302/10/1022, P302/12/G157; Grant sponsor: Ministry of Education Youth and Sports of the Czech Republic; Grant number: LD11020.

*Correspondence to: Eva Bártová, Institute of Biophysics, Academy of Sciences of the Czech Republic, v.v.i., Královopolská 135, CZ-612 65 Brno, Czech Republic. E-mail: bartova@ibp.cz

Manuscript Received: 11 January 2012; Manuscript Accepted: 22 May 2012

Accepted manuscript online in Wiley Online Library (wileyonlinelibrary.com): 29 May 2012

DOI 10.1002/jcb.24208 • © 2012 Wiley Periodicals, Inc.

2011]. In interphase nuclei, these CTs are separated by interchromatin channels that not only pervade the CTs, but also expand into their very interiors [Cremer et al., 1982; Cremer and Cremer, 2001; Lanctôt et al., 2007; Cremer and Cremer, 2011].

More recently, a number of laboratories have tried to find a functional relationship between nuclear architecture and gene expression [Kurz et al., 1996; Francastel et al., 2000; Bártová et al., 2002; Williams et al., 2002; Wiblin et al., 2005]. Consequently, the theory of chromosome territories and nuclear architecture has become a very important aspect of chromatin biology. Numerous studies have shown that CTs and their genomic sub-regions are arranged non-randomly within the interphase nuclei [Kozubek et al., 1999b, 2002; Parada and Misteli, 2002] and have a high degree of stability [Zink and Cremer, 1998; Chubb et al., 2002]. This means, for example, that when calculating the average radial distribution of gene-poor human chromosome 18 (HSA18) and gene-rich HSA19, HSA18 is positioned closer to the nuclear periphery whereas HSA19 is one of the most interiorly located chromosomes [Croft et al., 1999]. Restricted movement of chromosome sub-regions can be detected during physiological processes such as cell cycle progression or cell differentiation [Chaly and Munro, 1996; Bártová et al., 2000; Essers et al., 2005]. Specific reorganization of chromosomal sub-regions can also accompany pathophysiological processes, including malignant cell transformation or loss of A-type lamin function [Kozubek et al., 1997; Parada et al., 2002; Taslerová et al., 2003; Galiová et al., 2008; Meaburn et al., 2009]. For example, nuclear positions of fusion genes are determined by the final structure of the derivative chromosomes [Taslerová et al., 2003]. In addition, the close proximity of chromosome territories following exposure to ionizing radiation increases the probability of chromosome translocation [Kozubek et al., 1997; Nikiforova et al., 2000; Parada et al., 2002] and laminopathy-related cells are characterized by changes in heterochromatin formation and condensation of chromosome territories [Galiová et al., 2008].

This interest in CTs has also raised the question of whether the chromatin pattern defined by CTs is transmitted from mother to daughter cells. This question has been addressed by several studies with contradictory results [Gerlich et al., 2003; Walter et al., 2003; Thomson et al., 2004; Cvačková et al., 2009; Strickfaden et al., 2010]. For example, Gerlich et al. [2003] reported that global chromosome positioning is transmitted through the cell cycle, whereas Walter et al. [2003] documented that the arrangement of CTs is stable from mid-G1 to late-G2 cell cycle phases, but changes occur when the cells proceed through mitosis. This was supported by data of Cvačková et al. [2009], who pointed out the importance of stochastic components associated with rearrangement of CTs. Strickfaden et al. [2010] claimed that a combination of rotational and locally constrained CT movement can also influence the global arrangement of chromatin.

To address the question of whether the nuclear pattern is passed down through cell generations, we investigated chromatin arrangement in living cells. We focused particularly on heterochromatin, which is thought to be responsible for the protection of chromosome integrity [Grewal and Jia, 2007]. For these experiments we used photoconvertible histone H4–Dendra2 and mapped heterochromatin according to the presence of heterochromatin protein 1β (HP1β) tagged by green fluorescent protein (GFP). We also analyzed whether there is similarity in the chromatin arrangement and formation of HP1β foci or Cajal bodies in sister cells. Moreover, the degree of sister cell similarity was tested with respect to arrangement of nucleoli, selected chromosome territories, regions of increased gene expression (RIDGEs), regions of low gene expression (anti-RIDGE regions), and c-myc gene transcription sites. We also aimed to reveal how histone hyperacetylation or suppression of transcription can trigger chromatin rearrangement during interphase.

MATERIALS AND METHODS

CELL CULTIVATION AND TREATMENT

HepG2 cells that stably express H4–Dendra2 were a generous gift from Prof. Ivan Raška and Dr. Zuzana Cvačková (Charles University in Prague, First Faculty of Medicine, Prague, Czech Republic). The establishment of H4–Dendra2 HepG2 cells was described by Cvačková et al. [2009]. These cells were cultivated in Dulbecco's modified Eagle's Medium (PAN, Germany) supplemented with 10% fetal calf serum (PAN), 100 i.u./ml penicillin, and 0.1 mg/ml streptomycin. Cell cultures were maintained at 37°C in a humidified atmosphere containing 5% CO_2. This culture was used for living cell observations. HepG2 cells are adherent epithelial-like cells that grow as monolayers in small aggregates. In comparison with primary cell cultures with a diploid genome, HepG2 cells are characterized by a chromosome number of 55. HepG2 cells originated from the liver tissue of a patient with differentiated hepatocellular carcinoma and secrete plasma proteins, including albumin, transferrin, fibrinogen, α-2-macroglobulin, and plasminogen (http://hepg2.com).

In this study, we treated HepG2 cells with 100 nM trichostatin A (TSA) (Sigma-Aldrich, St. Louis, MO) or 0.5 μg/ml actinomycin D (#A9415, Sigma-Aldrich) for 2–5 h.

DNA repair events, potentially induced by the photoconversion by UV laser, were inhibited by addition of 10 mM hydroxyurea [Martin et al., 1999]. Hydroxyurea was not removed from the cultivation medium during cell observation.

In some experiments, cells were synchronized by a double thymidine block [Hofer et al., 2011] and changes in the cell cycle were measured by flow cytometry as described by Bártová et al. [2000]. In brief, 3 mM thymidine was added to growing HepG2 cells for 16 h and the adherent cells were washed with PBS. The cells were allowed to grow for 10 h in standard medium before a second addition of thymidine. After incubation for 16 h (taken as time 0), the cells were washed again with PBS and cultivated in standard medium. Cells were sampled at 2 and 5 h.

The nuclear arrangement of chromosome territories and gene transcripts in sister cells were studied in human adenocarcinoma HT29 cells that were cultivated according to Harničarová et al. [2006].

3T3 cells stably expressing GFP-HP1β were a generous gift from Dr. Paul Verbruggen from Swammerdam Institute for Life Sciences, University of Amsterdam (The Netherlands). Cells were cultivated according to Šustáčková et al. [2012a].

Mouse GOWT1 embryonic stem cells (mESCs) stably expressing OCT4 protein were a generous gift from Dr. Hitoshi Niwa (Laboratory

for Pluripotent Stem Cell Studies, RIKEN Center for Developmental Biology, Japan) and were cultivated according to Šustáčková et al. [2012b].

WESTERN BLOT ANALYSIS AND FLOW CYTOMETRY

Western blot analysis was performed following the procedure of Harničarová et al. [2006] using antibody against histone H4 (#ab10158, Abcam, UK). Analysis by flow cytometry was performed following Bártová et al. [2000].

DENDRA2 PHOTOCONVERSION AND LIVE CELL STUDIES

For these experiments we used a confocal microscope (Leica TSC SP5 X) equipped with white light laser (WLL; 470–670 nm in 1-nm increments), argon laser (488 nm), and two ultraviolet (UV) lasers (405 and 355 nm). An oil immersion objective with 63× magnification and numerical aperture (NA) of 1.4 was used. HepG2 cells were grown on glass-bottomed dishes (#P50G-0-30-F, MatTek Corporation, Ashland, MA), which were placed in a cultivation hood (EMBL, Heidelberg, Germany) maintained at 37°C and 5% CO_2 for experiments. Non-activated Dendra2 was visible as green fluorescence, monitored by WLL. Photoconversion of Dendra2 was induced by UV laser (405 nm) and photoconverted H4–Dendra2 exhibited red fluorescence, visualized by 561 nm WLL. For better contrast, photoconverted H4–Dendra2 is shown in blue in the figures. Experiments were performed in non-synchronized cells that were monitored every 5–10 min for 2–5 h after treatment with TSA or actinomycin D. The live mode of LEICA LAS AF (version 2.1.2.) software was used for long-term observation of cells over 24–48 h. In this way, we obtained information on how the cells pass through the cell cycle and could monitor patterns of transmitted chromatin in daughter, granddaughter, and sister cells. To study transmission of chromatin from mother to daughter cells, we performed H4–Dendra2 photoconversion at the nuclear periphery, closer to the nucleoli, and in half of the nucleus. We used the time-lapse imaging mode from LEICA LAS AF software for long-term observation of live cells.

IMMUNODETECTION

The potential phototoxic effect of the UV laser was investigated by immunodetection of phosphorylated histone H2AX (γH2AX), 53BP1, and cyclobutane pyrimidine dimers (CPDs), which represent markers of chromatin with DNA lesions [Fernandez-Capetillo et al., 2004]. For these analyses, cells were additionally irradiated with 5 Gy of γ-rays (Cobalt-60). Immunodetection was performed according to Bártová et al. [2005, 2008] using rabbit polyclonal antibody against γH2A.X (phospho S139; Abcam, #ab2893), 53BP1 (Abcam, #ab21083), and CPDs (Cosmo Bio Co., Ltd, Japan, #NMDND001) (Fig. 1). The nuclear pattern of Cajal bodies in sister cells was studied using antibody against Coilin (Santa Cruz Biotechnology, USA, #sc-32860).

ANALYSIS OF CHROMATIN REGIONS BY H4–DENDRA2 PHOTOCONVERSION

To test the effects of TSA and actinomycin D on chromatin, we selected a circle of 2-μm diameter for general H4–Dendra2 photoconversion within randomly selected regions of the nucleus. To identify heterochromatin, an area of 1-μm diameter around HP1β foci was selected prior to scanning. The fluorescence intensity and volume of photoconverted H4–Dendra2 area were calculated using FISH 2.0 software [Kozubek et al., 1999a, 2001]. In this way, we were able to study how selected agents affect chromatin condensation and positioning. Data from the FISH 2.0 analysis were exported to Sigma Plot 8.0 software (Jandel Scientific, CA), which was used to perform statistical analysis, including Student's *t*-test. All data in bar charts are expressed as mean ± standard error of the mean (SEM).

ANALYSIS OF SISTER CELLS

Fixed sister cells were identified based on identical nuclear shape and their position on microscope dishes or slides. We are aware that such visual detection of sister cells, especially in fixed material, does not represent a high-throughput analysis, but it is inherently likely that the cells are sisters when they are in close proximity and have similar nuclear shape. During live cell observation, sister cells were identified immediately after mitosis and then analyzed.

We additionally evaluated the sisterhood of cells by defining meaningful descriptors based on cell shape and texture and then studying the similarity of these descriptors in a database of nucleus images. The database contained 159 grayscale images of cell nuclei, out of which 87 were in live cells and 62 in fixed cells. The live cells were annotated, and therefore, we knew the sisterhood of all sister cells. The database contained 23 pairs of live sister cells (see Supplement 1).

We computed descriptors based on image texture, namely local binary patterns (LBP) [Ojala et al., 1996] and Haralick features (HARA) [Haralick, 1979], and on the shape of image structures. For this, we computed a granulometric curve (GR) [Soille, 2004], which expresses the distribution of structures of different size in the image, and used circular structuring elements to build granulometry curves. In order to eliminate the different cell sizes we normalized the grayscale granulometric curve by the granulometric curve of the nucleus binary mask.

We combined the descriptors and formed four vectors (denoted as LBP, GR, LBP + GR, and HARA + GR). Each vector is a marker of different properties (texture, granulometry, or their combination) for each database image. We measured the similarity of images as the distance between the description vectors using the standard L1 norm. In this way we could retrieve the nine most similar images for each nucleus in the database. In Supplement 1, we show for each live cell, the rank of her sister and their distance with respect to the four description vectors. Similarity with respect to our descriptors was confirmed in the majority of live sister cells; see http://cbia.fi.muni.cz/projects/sisters-JCB-2012.html.

FLUORESCENCE IN SITU HYBRIDIZATION (FISH)

Cells grown on slides were fixed with 4% (w/v) formaldehyde (Sigma, Czech Republic) dissolved in PBS (three-dimensional fixation). Cell fixation and DNA-FISH procedure was performed according to Strašák et al. [2009]. For the whole chromosome painting probe (HSA11), denaturation was performed at 70°C for 10 min and annealing at 37°C for 30–60 min. DNA/DNA hybridization proceeded overnight at 37°C. Post-hybridization washing was

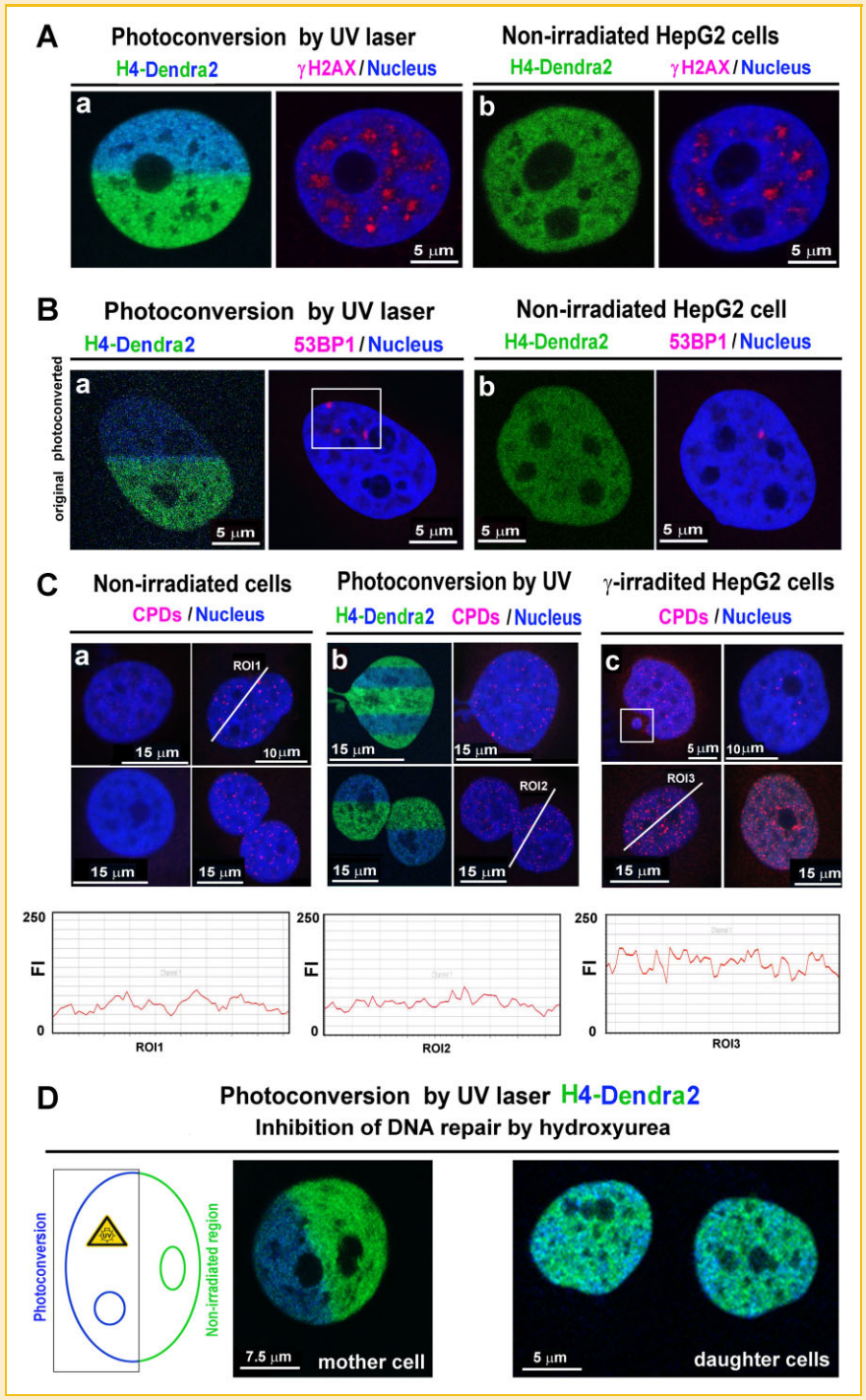

Fig. 1. Induction of DNA lesions by UV laser (405 nm) used for Dendra2 photoconversion. A: Nuclear pattern of γH2AX (red) in (a) UV irradiated HepG2 cell, and (b) non-irradiated cells. Irradiated cells were located according to coordinates marked on microscope dishes and the identity of given cells was verified according to the arrangement of surrounding cells. B: The effect of UV laser (405 nm) on chromatin structure and induction of DNA lesions was examined using antibody against: 53BP1 (red) in (a) UV-irradiated and (b) non-irradiated cells. C: Detection of anti-cyclobutane pyrimidine dimers (CPDs) (red) in (a) non-irradiated cells ($n = 100$), (b) cells irradiated individually by UV (number of cells analyzed $n = 15$), (c) γ-irradiated cells (whole cell population was irradiated; $n = 100$). Fluorescence intensity (FI) across selected ROIs was analyzed using LEICA LAS AF (version 2.1.2.) software. D: Transmission of nuclear pattern between mother and daughter cells when DNA repair was inhibited by hydroxyurea in living cells. Scale bars are shown in each panel.

performed according to Strašák et al. [2009]. DNA probes for RIDGE and anti-RIDGE regions of HSA11 were generated in the laboratory of Prof. Roel van Driel (University of Amsterdam, Swammerdam Institute for Life Sciences) using degenerate oligonucleotide primer-polymerase chain reaction (DOP-PCR) [Goetze et al., 2007]. Purified DNA was labeled using the digoxigenin (DIG)- or BIOTIN-Nick Translation Mix (Cat. Nos. DIG-1745816 and BIOTIN-1745824, Roche, Prague, Czech Republic). To pre-hybridize or competitively hybridize repetitive elements that would otherwise cause non-specific hybridization, we used human COT-1 DNA (#1581074, Roche). By dual color staining we were able to simultaneously study both HSA11 and RIGDE (anti-RIDGE) regions mapped on HSA11. For visualization we used Rhodamine-anti-DIG (Roche) and fluorescein isothiocyanate-conjugated-avidin (Roche). TO-PRO-3 iodide (0.04 μg/ml) was used as a counterstain. Image acquisition was performed using a Nipkow-disk based confocal microscope [Bártová et al., 2008; Strašák et al., 2009]. To detect the c-myc gene transcripts, we carried out a RNA-FISH procedure as described by Harničarová et al. [2006] or Bártová et al. [2008].

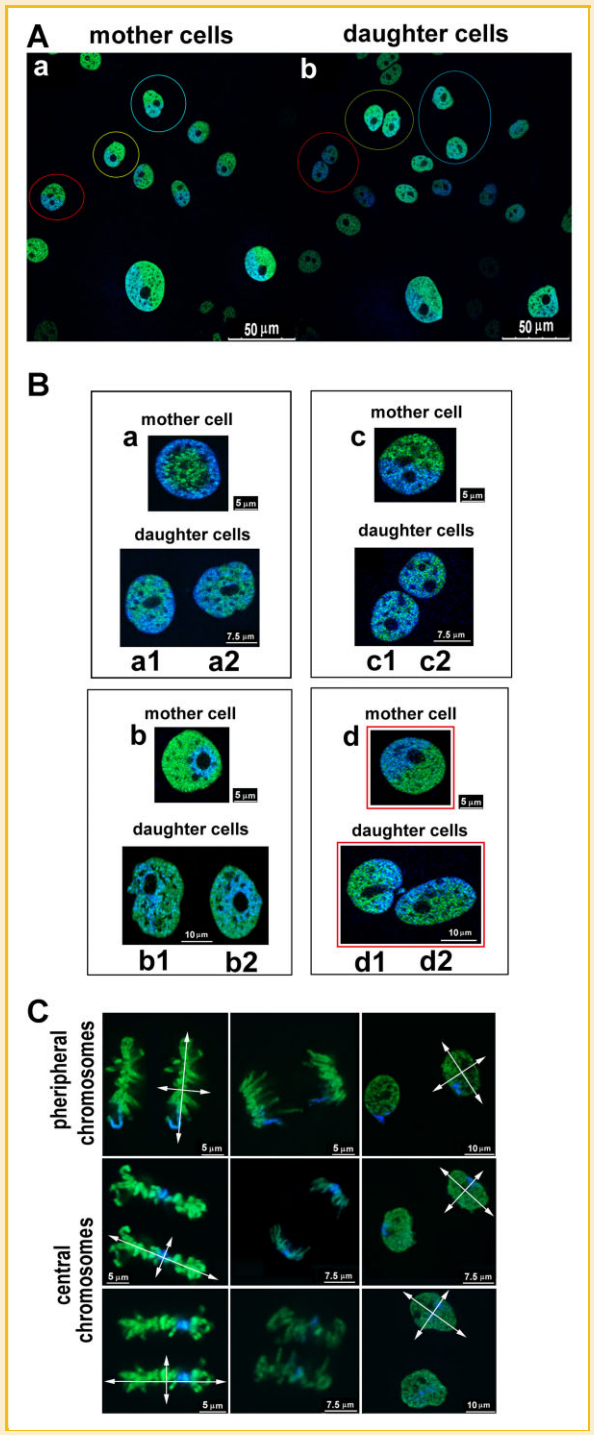

QUANTITATIVE ANALYSIS OF IMAGES

We used the following algorithm for quantitative analysis of the images shown in Figures 2B and 3A and compared the results using the Pearson correlation coefficient r_{xy} [Spiegel, 1992], which is widely used as a measure of linear dependence between two variables X_i and Y_i:

$$r_{XY} = \frac{\sum_{i=1}^{n} (X_i - \bar{X})(Y_i - \bar{Y})}{\sqrt{\sum_{i=1}^{n} (X_i - \bar{X})^2 \sum_{j=1}^{n} (Y_j - \bar{Y})^2}} \quad (1)$$

where $\overline{X}$ and $\overline{Y}$ are mean values of the corresponding variables X_i and Y_i. The standard error of the correlation coefficient is calculated as follows [Spiegel, 1992]:

$$\overline{m}_r = \sqrt{\frac{1 - r_{xy}^2}{n - 2}} \quad (2)$$

In our algorithm the variables X_i and Y_i are the intensities of the blue and the green colors at the same point (the same pixel) of the image, and "n" is the total number of pixels in the image.

We suggest that a quantitative measure of the similarity of images is the difference in their correlation coefficients (also taking into account the standard error of the coefficients): the closer the correlation coefficient is to 1, the more similar is the blue and green fluorescence spatial distribution.

Fig. 2. Transmission of photoconverted H4–Dendra2 from mother to daughter cells. Aa–Ab: H4–Dendra2 in interphase nuclei was photoconverted from green fluorescence to red fluorescence (shown as blue). The arrangement of photoconverted regions within interphase nuclei was studied. B: Panels a–d show photoconversion of H4–Dendra2 in mother cells. B: Panels a1–a2, b1–b2, c1–c2, d1–d2 represent transmission of photoconverted chromatin to daughter cells. H4–Dendra2 photoconversion was performed as follows: (Ba) at nuclear periphery, (Bc, Bd) in half of the nucleus, and (Bb) closer to the nucleoli. The area of photoconverted regions and ratio of green/blue signals was quantified and the results are shown in Table II. Cells in panel A,B were monitored for 24 h. C: Photoconversion in mitotic chromosomes. Lines were interlaid along the long axes of mitosis and long axes of interphase nuclei. The point of intersection was used to describe chromosome orientation. Chromosomes in the "very periphery of mitosis" or interphase nucleus (the longest distance from the point of intersection) and in mitosis "interior" or interphase nucleus interior (in close proximity to the point of intersection) were distinguished. Mitoses were monitored for 1.5 h. Scale bars are shown in all panels.

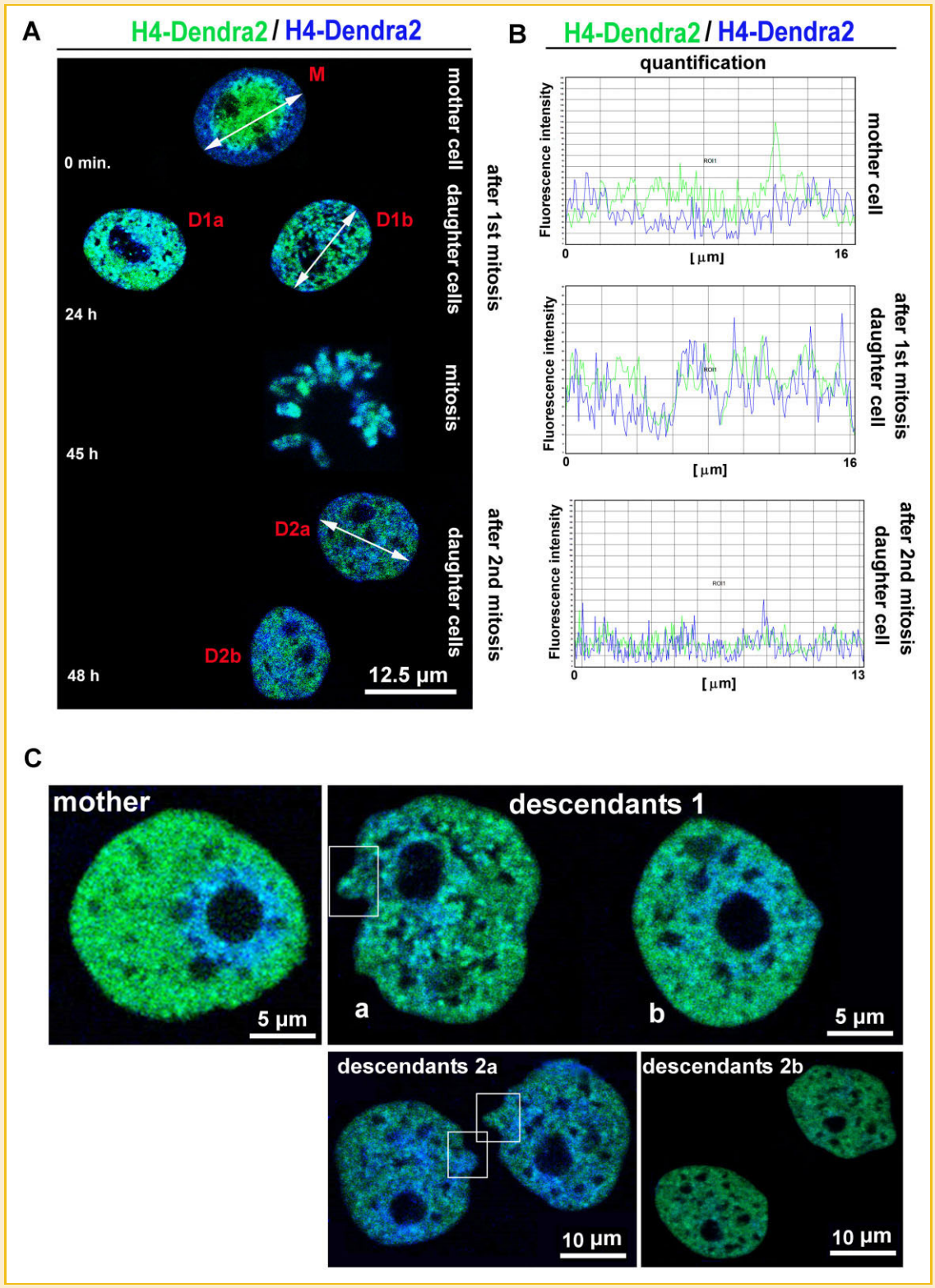

Fig. 3. Chromatin transmission after the first and second mitosis. A: Photoconversion of H4–Dendra2 at the nuclear periphery is shown in the mother cell (M). After the first mitosis (A-D1a, A-D1b), the chromatin pattern was not transmitted. When the cells passed through the second mitosis (A-D2a, A-D2b), photoconverted and non-photoconverted chromatin was mixed. Bar represents 12.5 µm. B: Quantification of H4–Dendra2 fluorescence (green) and photoconverted H4–Dendra2 (blue) in mother cell and after the first and the second mitosis. Quantification was performed using LEICA LAS AF (version 2.1.2.) software. The intensity of fluorescence of non-photoconverted H4–Dendra2 (green) and photoconverted H4–Dendra2 (blue) was analyzed according to selected regions of interest (ROIs) represented by a line across the whole nucleus (white arrow-headed line across the nuclei in panel A). The length of this line (in µm) is shown as the *x*-axis in relevant graphs. C: Nuclear pattern in mother cell and descendent 1 (a, b), and descendent 2 (2a, 2b) cells. Cell protrusions were observed in both descendents 1a, 1b and 2a, 2b (frames). Cells were monitored for 48 h.

CELL TRANSFECTION

Plasmid encoding red fluorescent protein (RFP)-proliferating cell nuclear antigen (PCNA) [Sporbert et al., 2005] was a generous gift from Prof. M. Cristina Cardoso (Technische Universität Darmstadt, Germany). HepG2 cells were transfected by plasmid encoding GFP-HP1β (#17651, Addgene, USA). The plasmids were transformed into *E. coli* DH5α and plasmid DNA was isolated using the QIAGEN Plasmid Maxi Kit (#121693, Bio-Consult, Czech Republic). Five micrograms of plasmid DNA was used for transfection of HepG2 cells with the METAFECTENE^{TM}PRO system (Biontex Laboratories GmbH, Germany).

RESULTS

NUCLEAR ARRANGEMENT OF PHOTOCONVERTED H4–DENDRA2 AFTER THE FIRST MITOSIS

The transmission of chromatin patterns was investigated in HepG2 cells that stably express photoconvertible histone H4–Dendra2. For these experiments we used green-to-red photo-switchable fluorescent Dendra2 derived from octocoral *Dendronephthya* sp. [Gurskaya et al., 2006]. The original H4–Dendra2 is shown in green (Fig. 1). After photoconversion to red fluorescence by UV irradiation, we used software to select a blue color for better contrast between the original and photoconverted H4–Dendra2.

Because UV radiation induces DNA lesions [summarized by Nagy and Soutoglou, 2009], we examined the effect of UV irradiation (laser line 405 nm) on chromatin stability in HepG2 cells. We analyzed the appearance of DNA lesions using antibodies against γH2AX and 53BP1 (Fig. 1A,B) and the induction of cyclobutane pyrimidine dimers (CPDs) as a marker of DNA damage (Fig. 1C) [Rogakou et al., 1998; summarized by Nagy and Soutoglou, 2009]. By immunofluorescence analysis, we documented the appearance of γH2AX-positive foci, considered markers of double strand DNA breaks [Nagy and Soutoglou, 2009]. γH2AX-positive DNA lesions were formed to the same extent in irradiated and non-irradiated cells (compare Fig. 1Aa,Ab). However, when we analyzed DNA lesions by staining for 53BP1, we found an approximately threefold increase in the number of 53BP1-positive foci in UV-irradiated regions then in non-irradiated counterparts (compare irradiated cells in Fig. 1Ba with non-irradiated cells in Fig. 1Bb). In the case of CPDs, we did not observe differences between non-irradiated and UV-irradiated cells (Fig. 1Ca,Cb; see fluorescence intensity across selected region of interest [ROI]). However, γ-irradiation by Cobalt-60 caused pronounced CPD positivity in the entire genome (Fig. 1Cc; note fluorescence intensity across selected ROI). Moreover, approximately 20% of γ-irradiated cells were characterized by formation of micronuclei (Fig. 1Cc, frame).

Despite the fact that Strickfaden et al. [2010] did not find any DNA damage after photoactivation of fluorochromes, we have observed increased 53BP1 positivity in UV-irradiated chromatin (see frame in Fig. 1Ba). However, when we inhibited DNA repair with 10 mM hydroxyurea [Martin et al., 1999] we did not observe distinctions in chromatin transmission when we compared the data with or without addition of hydroxyurea (compare Fig. 1D with Fig. 2A,B). Based on these results, we can exclude an effect of DNA repair events on chromatin pattern transmission between cell generations.

In the next experiment, we used a UV laser to photoconvert H4–Dendra2 positive chromatin at the nuclear periphery, the nuclear interior, and in only half of the nucleus (Fig. 2Aa,B). When the cells passed through mitosis, we monitored the nuclear pattern of the photoconverted regions (Fig. 2Ab). In 98% of cases, nuclear arrangement of chromatin was not identical in mother and daughter cells (compare Fig. 2Ba with a1 and a2, Fig. 2Bb with b1 and b2, or Fig. 2Bc with c1 and c2). A similar chromatin pattern between mother and daughter cells was observed for only ∼2% of events analyzed (compare Fig. 2Bd with d1 or d2; red frames). The number of cells analyzed and the occurrence of particular events are shown in Table IA.

To test whether there is a correlation between the two variables X_i (blue color after photoconversion) and Y_i (green color before

TABLE I. Number of Nuclei in the Evaluation

Nuclear event in mother cells	Number of mother cells	Total time of observation, hours	Pairs of daughter cells with transmitted nuclear pattern	Pairs of daughter cells without transmitted nuclear pattern
(A) Nuclear pattern in mother and daughter cells				
Photoconversion of nuclear periphery	20	24	0	20
Photoconversion of half of nucleus	20	24	1	19
Photoconversion of nucleolar periphery	15	24	0	15
(B) Nuclear pattern in mitotic chromosomes				
Number of mitosis studied				15
Evaluation period				1.5 h
(C) Number of sister cells studied to evaluate similarities in nuclear pattern				
Sister cells[a] with identical pattern of RIDGEs/anti-RIDGES in HSA11				52/48
Sister cells[a] with different pattern of RIDGEs/anti-RIDGES in HSA11				12/15
Total number of analyzed cells with stained RIDGE/anti-RIDGES				208/150 (number also involves cases when it was not possible to recognize sister cells exactly)
Sister cells[a] with identical pattern of c-myc transcripts				34
Sister cells[a] with different pattern of c-myc transcripts				5
Total number of analyzed cells with stained c-myc transcripts				191 (number also involves cases when it was not possible to recognize sister cells exactly)

[a]As sister cells were considered the cell nuclei with identical shape and located in close proximity.

TABLE II. The Correlation Coefficient Between the Blue and the Green Color Spatial Distributions

	r_{xy}	m_r
A: Analysis related to Fig. 2		
a	0.526	0.003
a1	0.846	0.002
a2	0.857	0.002
b	0.603	0.003
b1	0.9131	0.001
b2	0.9085	0.001
c	0.501	0.003
c1	0.871	0.002
c2	0.816	0.003
d	0.514	0.003
d1	0.704	0.003
d2	0.689	0.003
B: Analysis related to Fig. 3A		
M	0.681	0.006
D1a	0.961	0.003
D1b	0.953	0.003
D2a	0.950	0.003
D2b	0.954	0.003

Quantitative comparison of images using the Pearson correlation coefficient r_{xy} that was used as a measure of linear dependence between two variables X_i (blue signals) and Y_i (green signals).

photoconversion), we calculated their linear dependence using the Pearson correlation coefficient r_{xy} (see the Materials and Methods Section). As shown in Table IIA, values of the correlation coefficient increased after mitosis to a different extent in different cells. For example, in the cells with a transmitted nuclear pattern, the differences between correlation coefficients for the cell in Figure 2Bd and cells d1, d2 were 1.6- to 2-fold lower than those in cells with a non-transmitted nuclear pattern (see values in Table IIA for panels a,a1,a2 or b,b1,b2 or c,c1,c2). For a better explanation, we applied the following additional characterization rule: mother and daughter cells are classified as similar to each other (i.e., the arrangement of nuclear structures is transmitted through mitosis) if the difference in their correlation coefficients does not exceed the value of 0.2. For example, the calculation for Figure 2B is as follows: $r_{xy}(d1) - r_{xy}(d) = 0.704 - 0.514 = 0.19 < 0.2$; $r_{xy}(d2) - r_{xy}(d) = 0.689 - 0.514 = 0.175 < 0.2$ (Table IIA). However, for cells with a non-transmitted nuclear pattern after mitosis the calculation is $r_{xy}(c1) - r_{xy}(c) = 0.871 - 0.501 = 0.37 > 0.2$ (Table IIA).

In addition, in Figure 3A, the blue color spatial distribution was more similar between granddaughters (Fig. 3A-D2a,D2b) and daughters (Fig. 33A-D1a,D1b) than between daughters (Fig. 3A-D1a,D1b) and mother cells (Fig. 3A–M), in which the distribution of photoconverted chromatin was not similar (see correlation coefficient in Table IIB).

Next, we performed photoconversion of chromosomes in mitosis (Table IB) and addressed the question of how photoconverted chromosomes are integrated into interphase nuclei. In mitotic HepG2 cells that stably express H4–Dendra2, one chromosome was always photoconverted either on the periphery of mitosis or in the center of mitosis. Orientation of chromosome territories was established as follows: We interposed the straight line along the metaphase long axis and the second perpendicular axis. The point of intersection was a metaphase marker that was considered the center of mitosis. This served as a point from which we were able to set the orientation of photoconverted regions. The same was done for interphase nuclei (Fig. 2C). Here, we noticed that mitotic chromosomes positioned away from the point of intersection were mostly integrated into the periphery of interphase nuclei. Small mitotic chromosomes positioned in close proximity to the point of intersection were located in the interior of interphase nuclei or, when they appeared at the nuclear periphery, were associated with a compartment of the nucleoli (Fig. 2C). Taken together, these results confirm the observation of Bolzer et al. [2005] for flattened nuclei, namely that small chromosomes, independent of their gene density, were distributed significantly closer to the center of the nucleus or prometaphase rosette, while large chromosomes (in the Mb range) were located closer to the nuclear periphery or metaphase rosette rim.

NUCLEAR ARRANGEMENT OF PHOTOCONVERTED H4–DENDRA2 AFTER THE SECOND MITOSIS

In approximately 98% of cases, our data confirmed the results of Walter et al. [2003] and Cvačková et al. [2009] showing that global chromosome positioning is not transmitted from mother to daughter cells. In 2% of inspected cells, we observed the transmission of chromatin pattern during the cell cycle as described by Gerlich et al. [2003] (see Table IA). However, when we analyzed the nuclear pattern after the second mitosis, the chromatin arrangement was more similar to the chromatin pattern after the first mitosis (Fig. 3A and quantification in Fig. 3B). This may be because the initial chromatin order has been lost, and scrambled chromatin always looks much the same (compare cells in sections Fig. 3A-D1 with Fig. 3A-D2). Despite the fact that the H4–Dendra2 nuclear pattern was not transmitted from mother to daughter cells, certain similarities were observed in mother and descendent cell nuclei (Fig. 3C). For example, compare the protuberance in the frame of Figure 3C1a with nuclear protuberances in frames of descendent cells in Figure 3C2a. Moreover, sister cell nuclei in panel 2a resemble each other, similar to sister cell nuclei in panel 2b (Fig. 3C).

In our experimental model, we cannot exclude the possibility that deposition of "old" histones and integration of "old" and "new" histones into nucleosomes during replication or other chromatin-disturbing processes [Katan-Khaykovich and Struhl, 2011] might influence our view of nuclear pattern transmission. Although we suppose that the behavior of endogenous histone H4 is similar to that exogenous H4–Dendra2 (Fig. 4, inspect panel B), the possibility of random integration of "old" histones into the chromatin of daughter cells will always exist and is a limitation of our experimental model. For this reason, we additionally show that H4–Dendra2 mimics to some extent the behavior of endogenous histone H4 (Fig. 4). In this case, when we compared non-synchronized cells (Fig. 4Ae; ~72% in G1 phase of the cell cycle) with cells synchronized by double thymidine block (Fig. 4Ac; 73% blocked in G2 phase) (see Fig. 4Aa–e), we found a marked increase in the level of histone H4 and a slightly increased level of H4–Dendra2 in cells in G2 phase, compared with control cells in G1 (Fig. 4B). These experiments confirmed the expected cell cycle-dependent changes in the levels of both endogenous and exogenous histone H4; thus, reveal a limitation of our experimental model.

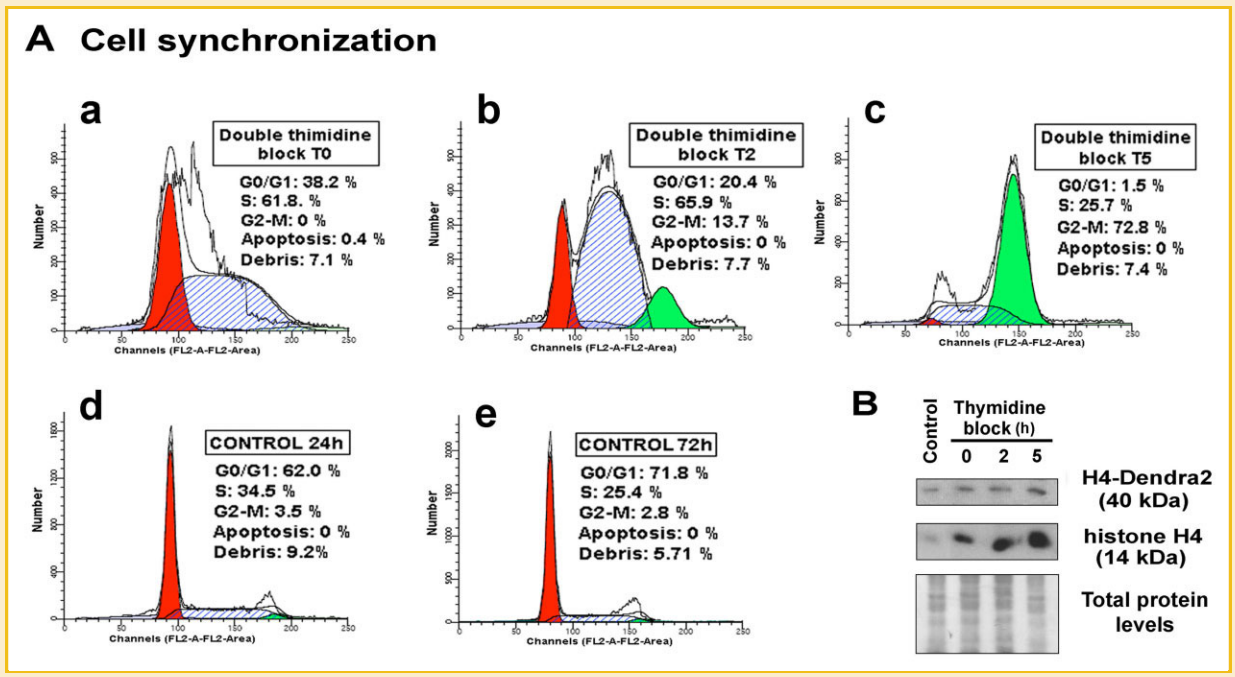

Fig. 4. Western blot analysis of levels of endogenous histone H4 and exogenous H4–Dendra2 during the cell cycle. A: Cell cycle profiles were measured using a FACS Calibur flow cytometer. G1 phase is shown as red, S-phase as dashed blue, and G2–M as green. Cells were synchronized by double thymidine block (panels a–c show cell cycle profiles at time [T] 0, 2 and 5 h after thymidine addition). Cell cycle profiles in panels a–c were compared with non-treated cells (d,e). ModFit software was used for cell cycle modeling. B: Levels of H4 and H4–Dendra2 were studied in non-treated and thymidine-treated cells. Non-treated (control) cells at 72 h cultivation were considered to be G1 cells (~72% of cells were in G1 phase; see panel e). At 5 h after the thymidine block, an increased H4 level was expected because of cell blockage in G2 phase (~73%, pane Ac). H4 and H4–Dendra2 levels were normalized to the total protein levels.

TRANSMISSION OF HP1β NUCLEAR PATTERN

We also tested whether there is similarity between the nuclear pattern of heterochromatin-related protein HP1β in mother and daughter cells (Fig. 5A1,A2) and found partial similarity, especially for foci associated with nucleoli (Fig. 5A1, frames). Moreover, in these cells the pattern of the nucleoli was very similar in mother and daughter cells, but the distances between nucleoli that are surrounded by HP1β foci were not identical in mother and daughter cells or in sister cells (Fig. 5A2). It is often hard to judge whether there is similarity in the HP1β arrangement in mother and daughter cells because of cell rotation. However, similar conclusions can be drawn from experiments in which we were able to identify cells in individual cell cycle phases based on the pattern of RFP-PCNA protein [Zolghadr et al., 2008; Fig. 5B]. In this way, we were able to distinguish S-phase and non-S-phase HepG2 cells expressing H4–Dendra2. Sister cells were identified by their similar nucleolar morphology (Fig. 5B, nuclei 1a, 1b and 2a, 2b) and the diffused RFP-PCNA pattern shows an identical cell cycle phase (non-S phase) in sister cells (Fig. 5B, lower right panel). Moreover, during the cell cycle we observed a nearly identical pattern of HP1β and nucleoli in cells blocked in S phase and those in non-S phase (Fig. 5C). Here, it is also evident that rotation of the nucleus can influence our assessment of nuclear arrangement (Fig. 5C). For example, when we horizontally rotated non-S phase cells, the similarity in nucleoli and HP1 β foci composition with S-phase cells was more evident (in Fig. 5C compare HP1β foci, labeled by numbers 1–4, and nucleoli, labeled by letters a–c).

NUCLEAR STRUCTURE IDENTITY IN SISTER CELLS

In these studies, we show symmetry in the nuclear pattern between sister cells. Sister cells were considered have nuclei of identical shape and be located in close proximity. For example, an identity in nuclear pattern was observed when we inspected the shape of nucleoli in sister cells after mitosis (see example in Figs. 2B, panels c1 and c2 or b1 and b2).

Since other nuclear structures, including RIDGEs and anti-RIDGEs, have been found to be important with respect to nuclear organization [Goetze et al., 2007] and gene expression [Caron et al., 2001; Versteeg et al., 2003; Gierman et al., 2007], we tested the nuclear distribution of chromosome 11 (HSA11) and related RIDGE or anti-RIDGE regions in fixed sister cells (see Fig. 6; frames in panel Fig. 6Aa show regions studied on HSA11). Sister cells were characterized by an identical pattern of these genomic regions (Fig. 6Ab,Ac): the arrangement of HSA11 and RIDGEs or HSA11 and anti-RIDGEs was identical in approximately 70–80% of sister cells (Table IC). The relevant chromosome territories were of similar shape, but in some cases there was variation in the degree of chromosome condensation or the distances between two chromosome territories in sister cells (compare chromosome condensation in Fig. 6Ab; chromosome territory 1 and 2 or distances a1–a2 with distances b1–b2 in Fig. 6Ac). We also measured the area of HSA11 (normalized to the nuclear radius) in sister cell nuclei and compared this parameter with the area of HSA11 in randomly selected pairs of cell nuclei (Fig. 6Ba,Bb). The graphs show a very similar area of HSA11 in sister cells (Fig. 6Ba), which was completely different from

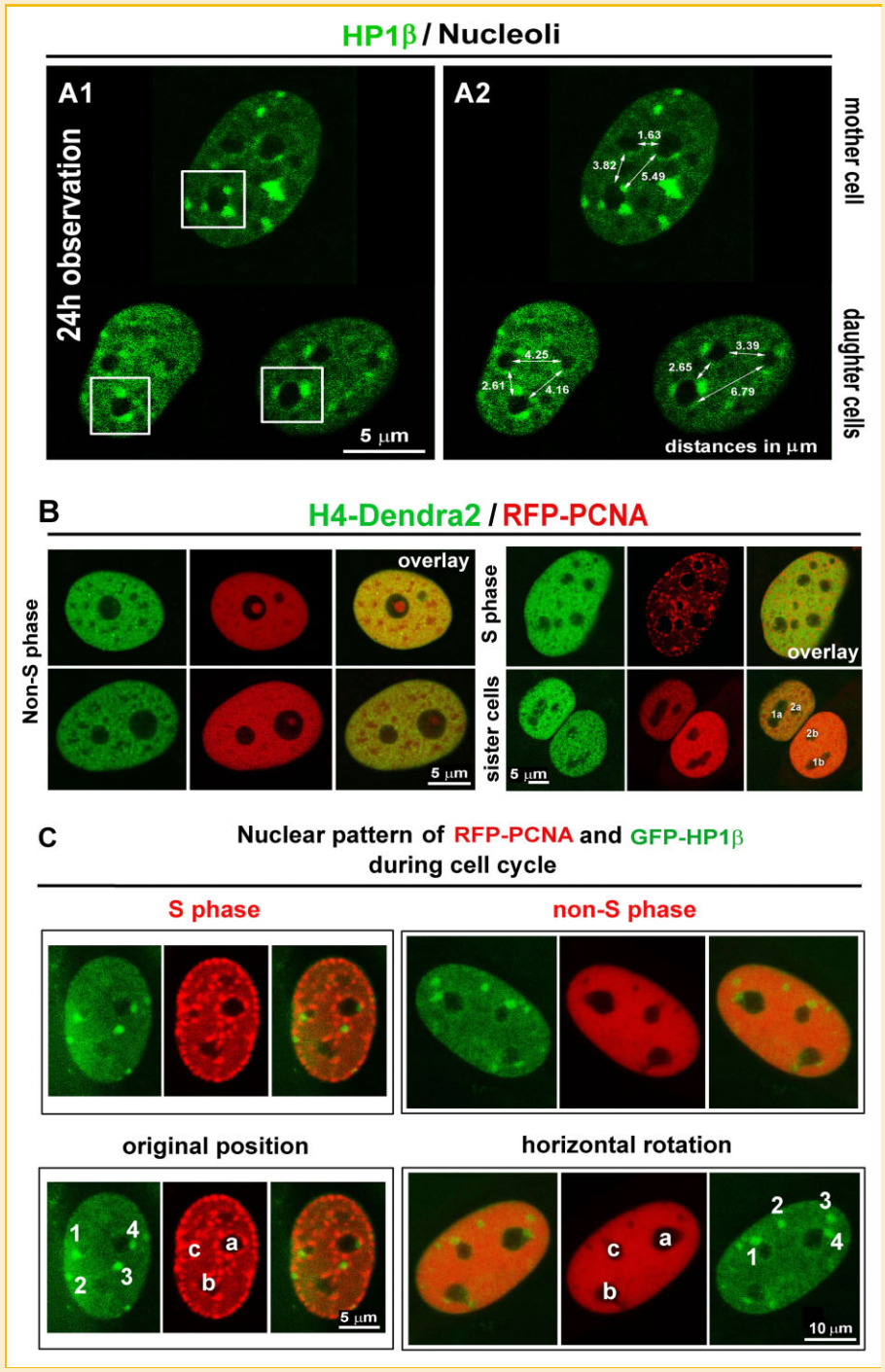

Fig. 5. Arrangement of nucleoli and HP1β foci in living cells. A1: Partial transmission of HP1β nuclear pattern from mother to daughter cells. The frames indicate HP1β pattern close to nucleoli, which were nearly identical in mother and daughter cells. A2: Distance between the nucleoli surrounded by HP1β was measured in mother and daughter cells. Analysis showed different distances between the nucleoli of mother and daughter cells. B: Nuclear pattern of RFP-PCNA (red) and H4-Dendra2 (green) in S-phase and non-S phase cells. C: Nuclear pattern of RFP-PCNA (red) and GFP-HP1β (green) in identical S-phase and non-S phase cell. Labels 1–4 show arrangement of HP1β foci in S-phase and non-S phase cells. Similarly, letters a–c show arrangement of nucleoli during the cell cycle. Scale bars are shown in μm for each panel.

data from randomly selected cell nuclei (Fig. 6Bb). Taken together, nuclear patterns of RIDGEs, anti-RIDGES, and whole territories of chromosomes 11 in sister cells are similar, but distances between individual chromosome territories are not identical.

Another interesting subject in chromatin biology is the nuclear arrangement of transcription sites [Harničarová et al., 2006; Takizawa et al., 2008]. We compared the c-myc gene transcription sites in sister cell nuclei and showed unambiguous identity in

nuclear positioning of the c-myc transcripts (Fig. 7A, Table IC). Analysis of nuclear radial distribution of the c-myc transcripts, as described by Harničarová et al. [2006], showed specific distribution of these transcription sites, with the majority of these regions positioned in the nuclear interior (Fig. 7A,Ba). Although in 10% of cell nuclei the c-myc transcription sites appeared very close to the nuclear periphery, the location of the c-myc transcripts in sister cells was again very similar (Fig. 7Aa). In the majority of sister cell nuclei, we have observed an identical distance of c-myc transcription sites from the nuclear weight center. This is documented by co-localization of red and green symbols in the circle diagram (Fig. 7Bb).

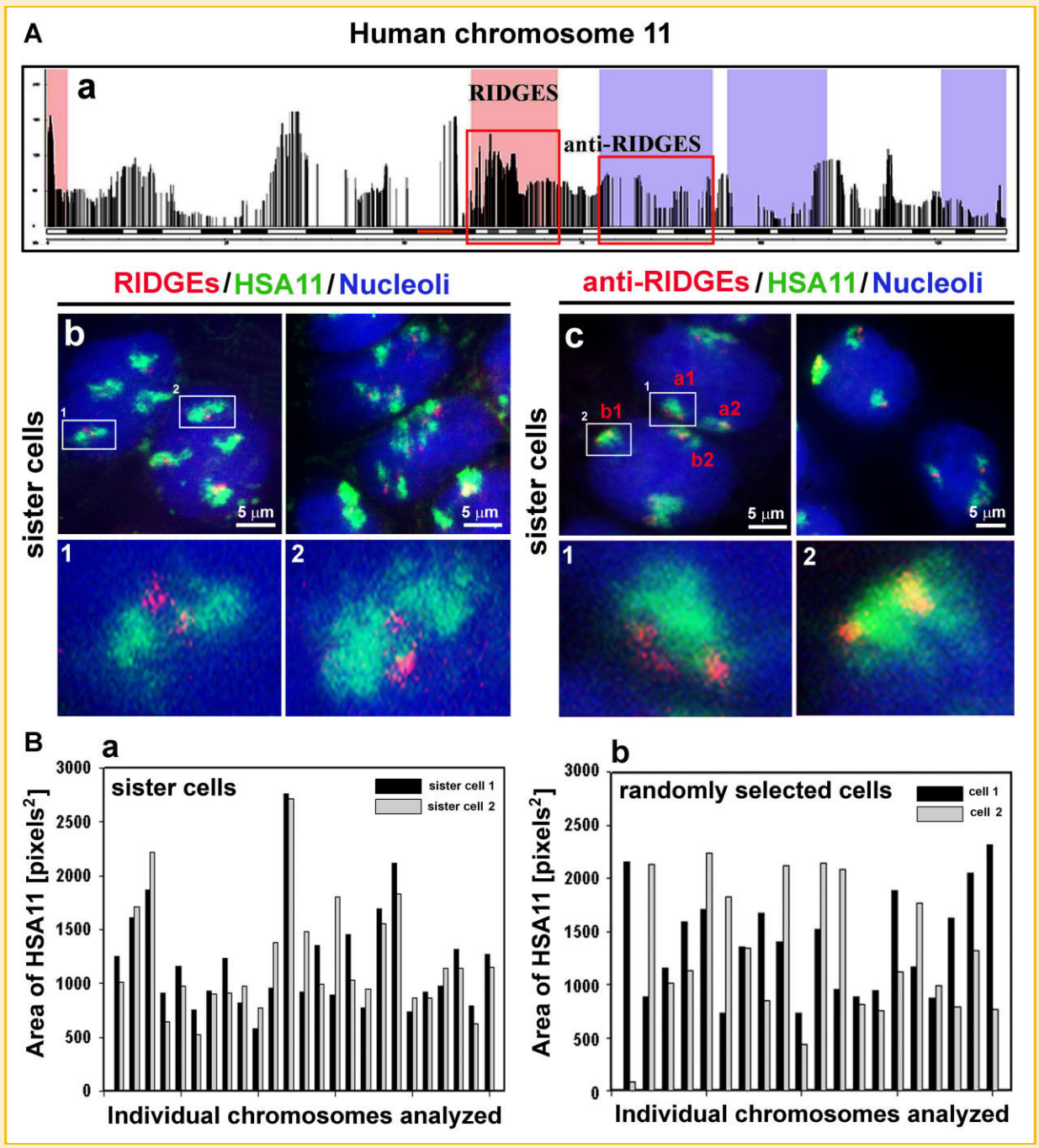

Fig. 6. Striking resemblance in HSA11 between HT29 sister cells. Aa: Regions of increased gene expression (RIDGEs; pink regions) and regions of low gene expression (anti-RIDGEs; blue regions) mapped on human chromosome 11 (HSA11). The studied RIDGEs and anti-RIDGEs are bordered by red frames. Ab: Similarity between sister cells in RIDGES (red) and HSA11 (green). Ac: Similarity between sister cells in anti-RIDGEs (red) and HSA11 (green). Frames 1 and 2 in panel Ab and Ac are randomly selected HSA11 with RIDGE (or anti-RIDGE) regions that look identical in sister cells and are magnified as 1 and 2 in the lower panels. Scale bars are shown in μm. Ba: Area of HSA11, normalized to the nuclear radius, in sister cell nuclei. Bb: area of HSA11, normalized to the nuclear radius, in randomly selected cell nuclei.

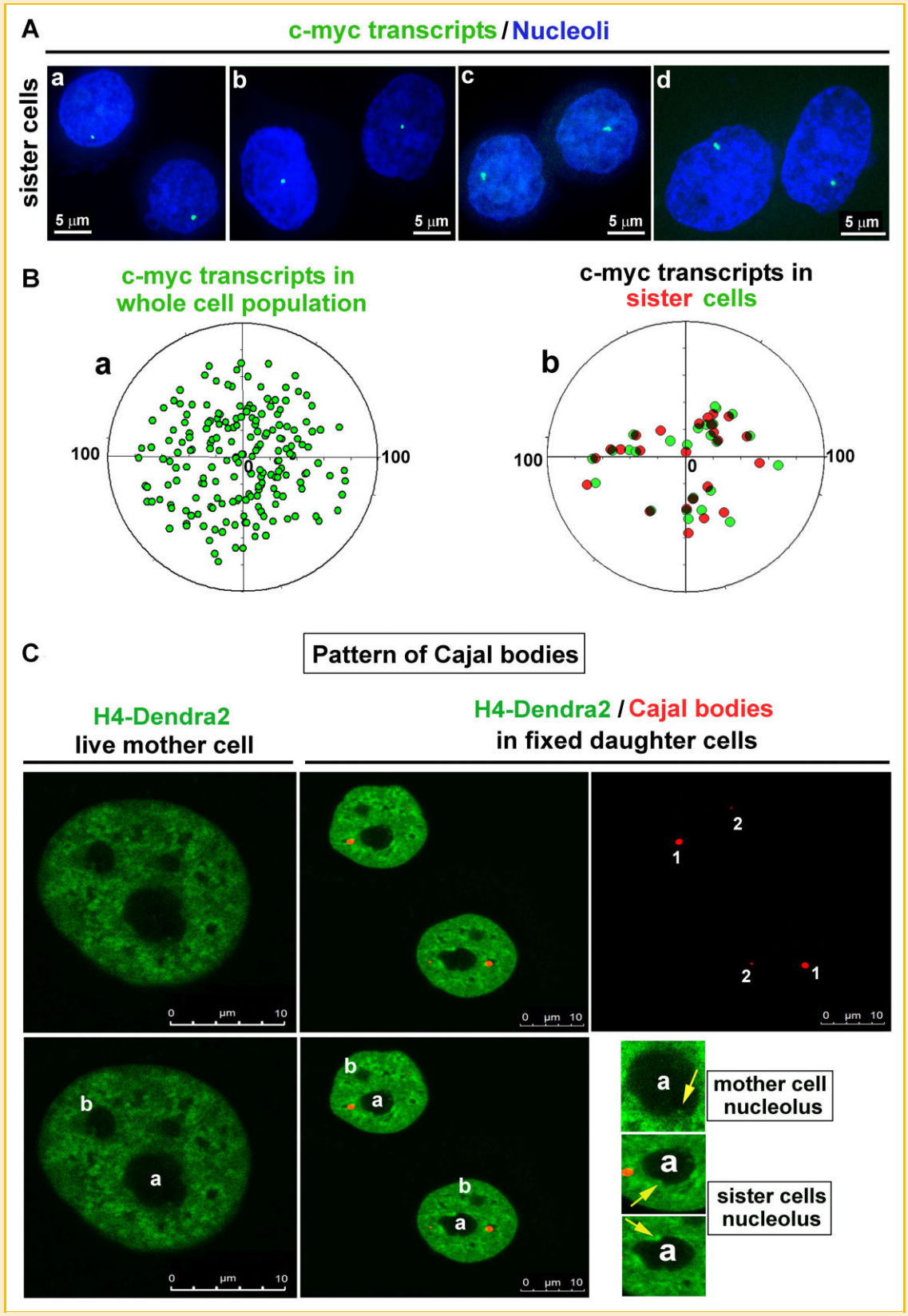

Fig. 7. Identity of sister cell nuclei. A: Identical nuclear location of the c-myc gene transcripts (green) in HT29 sister cell nuclei (blue). B: Analysis of nuclear distribution of the c-myc transcription sites in (a) whole cell population and (b) selected sister cells identified according to nuclear shape and position on microscope slides. C: Pattern of Cajal bodies in sister cell nuclei. The original mother cell nucleus, expressing H4–Dendra2 (green), is shown. By time-lapse microscopy it was possible to monitor mother cell division. The sister cells (green) were fixed after mitosis and the pattern of Cajal bodies (red) was determined. Individual Cajal bodies are numbered (1, 2) and coincident nucleoli are labeled by letters a, b. Within the nucleolar compartments, characteristic protrusions (yellow arrows) were visible in mother and both sister cells. Scale bars are shown in μm.

Nuclear pattern similarity in sister cells was confirmed by additional experiments. We monitored living cells expressing H4–Dendra2 and let these cells pass through mitosis. The position of sister cells was registered on microscope dishes and the cells were stained with antibody against Coilin [Cajal bodies, see Dundr, 2012]. We found that the nuclear pattern of Cajal bodies was almost identical in sister cell nuclei (Fig. 7C). In addition, the morphology of nucleoli was nearly identical in mother and both sister cells (see shape of nucleoli and protrusions in nucleoli in Fig. 7C, yellow arrows).

Similarity of sister cell nuclei was further tested by querying the cell database (see http://cbia.fi.muni.cz/projects/sisters-JCB-2012.html). We queried 10 the most similar images (9 + 1 tested cell) according to four descriptors (LBP, GR, LBP + GR, HARA + GR) and studied the rank and distance of the sister images (the complete answer is shown at http://cbia.fi.muni.cz/projects/sisters-JCB-2012.html). The meaningfulness of the descriptors is demonstrated in Supplement 1, where the sisterhood was known thanks to observing the living cells after mitosis. Here, we measured the similarity between mother cell (Fig. 7C) and her two daughters, studied by time-lapse confocal microscopy (see sisters in Fig. 7C or results in Supplement 2A). Our approach has demonstrated certain similarity between mother and her sisters but it was much lower than the similarity between sister cell nuclei (see rank values for sisters, id. 2 in Supplement 1). We applied the same approach for fixed cells. For example, Supplement 2 (B–E) shows similarity between two fixed sister cell nuclei from Fig. 7Aa–d. These nuclei were visually assumed as sisters and our approach also confirmed this statement. As example, the highest similarity in all parameters tested was found for sister cell nuclei (Fig. 7Ad) in Supplement 2, panel E (values 1/1 in all parameters).

HISTONE HYPERACETYLATION AND SUPPRESSION OF TRANSCRIPTION CHANGED THE DEGREE OF CHROMATIN CONDENSATION AND CAUSED REPOSITIONING OF PHOTOCONVERTED REGIONS DUE TO PRONOUNCED CELL ROTATION

When HepG2 cells stably expressing histone H4–Dendra2 underwent photoconversion by UV laser we observed pronounced rotation of whole nuclei during 2 h of observation, which likely caused a pronounced relocation of photoconverted chromatin (see direction depicted by arrows in Fig. 8A,E or movie 1). When we photoconverted H4–Dendra2 close to HP1β foci, we observed no changes in control cells during the period of observation (Fig. 8B). Hyperacetylation caused by TSA induced decondensation of chromatin, especially that associated with nucleoli (nuclear center), whereas less pronounced decondensation was observed in chromatin at the nuclear periphery (Fig. 8C, quantification in Fig. 8H compare a with b). Moreover, H4–Dendra2 photoconverted regions close to HP1β foci were decondensed 2 h after TSA treatment (Fig. 8D). This observation supports our recent findings that the HP1β trajectory and nuclear pattern can be influenced by inhibition of histone deacetylase [Bártová et al., 2005; Stixová et al., 2011].

For suppression of transcription we treated cells with actinomycin D. Actinomycin D treatment resulted in an enlarged interchromatin space (see black space in Fig. 8E; dark regions interlaced with H4–Dendra2 positive areas) and surprisingly caused decondensation of photoconverted regions, especially at the nuclear periphery (Fig. 8E and Fig. 8Hc,d). Prolonged exposure to actinomycin D was associated with cell squeezing but decondensation of photoconverted areas was maintained (Fig. 8F). Actinomycin D also caused relocation of photoconverted regions to the extreme nuclear periphery (Fig. 8E compared with Fig. 8F showing 90–140 min actinomycin D treatment). In this type of experiment, we also noticed pronounced rotation of the cells, which caused remarkable shifting of the photoconverted regions (see arrows in Fig. 8E or movie 1). Thus, based on these results we are aware that changes in the trajectory of photoconverted regions might be caused by whole cell rotation during interphase (movie 1). To test whether relocation of photoconverted areas is influenced by our experimental approach of 2D-scanning we also used a 3D-scaning mode and generated 3D projections of interphase nuclei of non-treated cells. In this case we also observed cell nuclei with pronounced rotation that appeared as relocation of photoconverted areas, even in lateral projections (compare z-projections in Fig. 8G, 0 min vs. 30 or 60 min). Moreover, 3D scanning caused bleaching of H4–Dendra2 and the fluorescence signals became weaker during the experiment (see Fig. 8G). Thus, this approach has limitations especially with respect to time-lapse microscopy.

DISCUSSION

Although many laboratories have studied the transmission of higher order chromatin structure during the cell cycle, the results to date are contradictory. Some studies showed that chromatin arrangement is transmitted from mother to daughter cells [Essers et al., 2005; Gerlich et al., 2003]. On the other hand, Walter et al. [2003] suggested that stability of chromatin arrangement is maintained during interphase, but major changes in the neighborhood chromosome territories (CTs) occur after mitosis. Ultimately, Essers et al. [2005] also admitted that similarity in chromatin arrangement between mother and daughter cell is not absolute, which is evident in the first figure of their paper. In further studies, Cvačková et al. [2009] and Strickfaden et al. [2010] claimed that distribution of chromatin differed from mother to daughter cell nuclei, but the CT neighborhood pattern established in the mother nucleus is not entirely lost after a single mitotic event. Thus, from the above findings, it is evident that distinct experimental approaches might influence the final results and interpretation of nuclear architecture. Strickfaden et al. [2010] discuss many aspects of cell-cycle-related chromatin arrangement that have been described since the initial observations of Boveri and suggest a new model of chromatin dynamics based on long-range DNA interaction in *trans* that places importance on mutual interaction of genes located on different chromosome territories.

Here, we addressed nuclear architecture in cycling cells that stably express histone H4–Dendra2 (Figs. 1–3 and 8). However, we are aware of the limitations of our experimental approach; for example, we must take into account the integration of "new" and "old" histones into newly synthesized chromatin [Katan-Khayko-

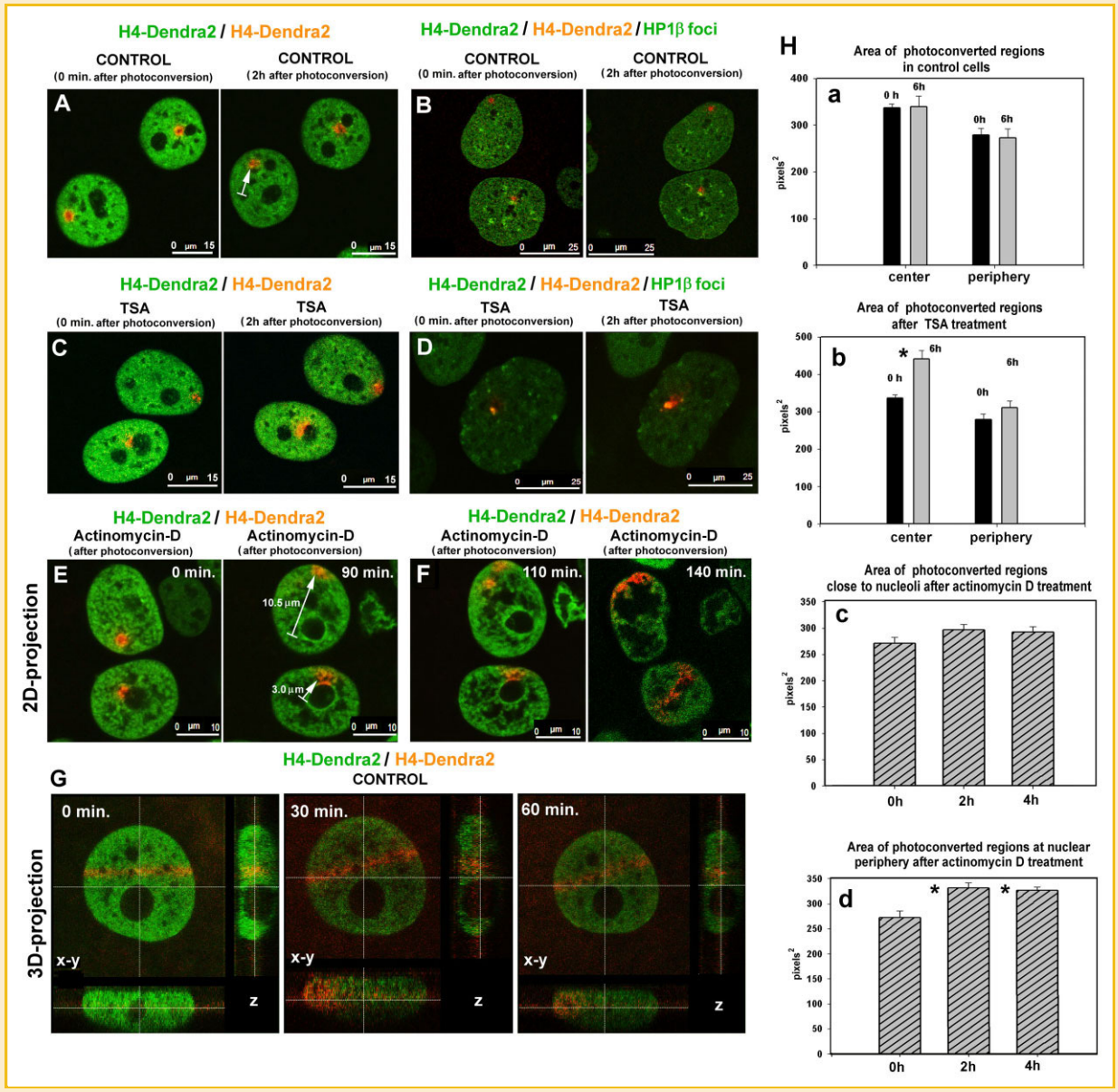

Fig. 8. Chromatin changes induced by TSA and actinomycin D treatment. Histone H4 Dendra2 was photoconverted close to the nuclear periphery, in close proximity to nucleoli and close to HP1β foci (HepG2 cells expressing H4–Dendra2 were transfected by plasmid encoding GFP-HP1β, Addgene, #17651). Live cells were monitored every 5–10 min for 120 min. A: Photoconverted H4–Dendra2 in control cells. B: Photoconverted H4–Dendra2 in close proximity to HP1β in control cells. C: Photoconverted H4–Dendra2 in cells treated with TSA. D: Arrangement of chromatin in close proximity to HP1β in cells treated with TSA. E: H4–Dendra2 photoconversion after actinomycin D treatment. Cell nuclei are shown in 2D-mode. F: Chromatin re-arrangement was monitored for 140 min after photoconversion of H4–Dendra2 in actinomycin D treated cells. G: 3D-projections of interphase nuclei of control non-treated cells. Photoconversion was performed in a defined ROI (red stripe). Scale bars are shown. H: Quantification of area of H4–Dendra2 after photoconversion in control and treated cells. In comparison with the control cell population (panel a), TSA (panel b) caused chromatin decondensation, especially when H4–Dendra2 was photoconverted in the nuclear interior (center). Actinomycin D (panels c and d) enlarged the photoconverted area, especially at the nuclear periphery (asterisks). The area of photoconverted H4–Dendra2 is shown in pixels^2 as mean ± standard error (SEM) and asterisks show statistically significant differences at $P \leq 0.05$.

vich and Struhl, 2011]. However, experimental approaches used in other studies also have limitations. Boveri's initial hypothesis on the maintenance of chromosome arrangement during interphase was later addressed by Strickfaden et al. [2010], who provided evidence for a persistent pattern in the proximity of CTs during interphase in selected cell types. However, they claimed that occasional cell rotation might influence the chromatin proximity pattern during interphase. Müller et al. [2010] suggested that the complex chromosome volume and morphology is fully established immediately after mitosis, but subtle changes in chromosome morphology appear after the first hour of G1 phase. Therefore, one must also take into account rotation of the cells or cell nuclei. For example, we found that re-arrangement of chromatin can be observed after actinomycin D treatment that additionally induces pronounced cell movement (see 2D- and 3D-projections of nuclei in Fig. 8E,G). Despite mentioned limitation of experimental approaches, living

cell studies, and especially application of photoconvertible fluorochromes, enable biologists to monitor and better understand long-standing processes, including cell cycle progression or differentiation.

In our experimental model based on H4–Dendra2 photoconversion, we noticed a very low percentage of daughter cells with a nuclear pattern similar to that of the parental cell (compare Fig. 2Bd-d1 or Bd-d2, red frames). Transmission of the nucleolar pattern seems to be somewhat clearer (Fig. 5A1), although distances between nucleoli are not identical (Fig. 5A2). Using our experimental approach, for the majority of maternal and descendent cells it was not possible to say that there is absolute similarity, only that some parts of the nucleus can be identical. However, the similarity in the composition of nucleoli in sister cell nuclei is much more striking (see example in Fig. 2Bc1 and c2 or Fig. 5B). Therefore, we can conclude that there is similarity in the pattern of nucleolar composition in sister cells (example in Fig. 7C, yellow arrows). This was observed despite the fact that photoconverted chromatin around the nucleolus was not found to be transmitted from mother to daughter cells [Cvačková et al., 2009].

We also tried to compare sister cell identity with respect to nuclear chromosome territory arrangement. Mirrored chromatin symmetry in sister cell nuclei is shown in Figure 6Ab,Ac; nearly identical nuclear pattern of HSA11 and related RIDGE and anti-RIDGE regions was found. Similarity in the pattern of sister cell nuclei was also observed for the c-myc transcription sites (Fig. 7A,B) and arrangement of Cajal bodies (Fig. 7C). Based on our observation that the majority of sister colon cancer cells are synchronized in c-myc transcription pattern (Fig. 7Aa–d), it seems to be evident that the result of cell division is not stochastic. Conversely, in embryonic stem cells (ESCs) asymmetric cell division, caused by tissue environment and cell-to-cell contact, was described [Hawkins and Garriga, 1998]. It is very interesting that asymmetric division of ESCs generates one cell with a similar transcription pattern to the mother pluripotent cell and one cell that differs in its expression profile and resembles a more differentiated phenotype. With this in mind, we have analyzed mouse ESCs in culture and in many cases have found cells with a similar nuclear shape and NANOG pattern within mESC colonies (see Supplement 3A, labeled cells). Moreover, time-lapse microscopy confirmed that sister cells have a similar nuclear shape (Supplement 3B). These data showed that nuclei of in vitro cultivated sister cells, even ESCs, have usually similar pattern.

Taken together, these findings suggest that chromatin has an enigmatic identity within the cell. Many studies indicate that the conformation of particular nuclear sub-compartments determines proper nuclear functions, including replication, transcription, splicing, and DNA repair. Here, we addressed whether the nuclear pattern is transmitted through mitosis or is identical in sister cell nuclei. We are aware that our results might be influenced by limitations of the methodology, especially when we used H4–Dendra2 photoconversion by UV laser. Although we excluded the possible influence of UV irradiation on our results (compare Fig. 1D and Fig. 2B), we must take into account the fact that H3–H4 histone tetramers associated with DNA can be unstable during replication, transcription, or other chromatin-disrupting processes [Katan-Khaykovich and Struhl, 2011]. Thus, many efforts are being directed towards the development and application of new methodologies, including advanced microscopy techniques such as stimulated emission depletion microscopy (STED), transmission electron microscopy (TEM), or chromosome conformation capture analyses (3C, 4C or Hi-C). These methods enable to reveal precisely the organization of chromatin or genome-wide chromatin interactions [Simonis et al., 2006; Wildanger et al., 2008; Lieberman-Aiden et al., 2009]. It will enhance our knowledge of chromatin plasticity, arrangement, and dynamics in the entire genome. In addition, these techniques will enable us to show how chromatin is functionally compartmentalized. It leads to better understanding of normal physiological processes and pathophysiological nuclear disorders.

ACKNOWLEDGMENTS

We thank Prof. Raška and Dr. Zuzana Cvačková (1st Faculty of Medicine, Charles University in Prague, Czech Republic) for HepG2 cells stably expressing H4–Dendra2. We additionally thank Dr. Paul Verbruggen (Swammerdam Institute for Life Sciences, University of Amsterdam, The Netherlands) for 3T3 cells stably expressing HP1β. The authors declare the following responsibility: Darya Yu Orlova and Lenka Stixová contributed equally to the experimental results. Stanislav Kozubek was responsible for financial support and he was the PhD supervisor of the first author. Hinco J. Gierman and Rogier Versteeg provided probes for RIDGEs and anti-RIDGE and critically read the manuscript. Gabriela Šustáčková and Soňa Legartová were responsible for optimization of the immunofluorescence technique. Andrei V. Chernyshev and Ruslan N. Medvedev performed statistical analysis. Pavel Matula and Roman Stoklasa designed software that enabled us to analyze sister cell similarity. Eva Bártová designed experiments, coordinated the efforts and wrote the paper. Our work was supported by following agencies: Grant Agency of Czech Republic, grant nos.: P302/10/1022; P302/12/G157 and by Ministry of Education Youth and Sports of the Czech Republic, grant no.: LD11020. EB is also a member of the EU COST action TD09/05 and principal investigator of EU Marie Curie project PIRSES-GA-2010-269156-LCS.

REFERENCES

Bártová E, Kozubek S, Kozubek M, Jirsová P, Lukášová E, Skalníková M, Buchníčková K. 2000. The influence of the cell cycle, differentiation and irradiation on the nuclear location of the abl, bcr and c-myc genes in human leukemic cells. Leuk Res 24:233–241.

Bártová E, Kozubek S, Jirsová P, Kozubek M, Gajová H, Lukášová E, Skalníková M, Ganová A, Koutná I, Hausmann M. 2002. Nuclear structure and gene activity in human differentiated cells. J Struct Biol 139:76–89.

Bártová E, Pacherník J, Harničarová A, Kovařík A, Kovaříková M, Hofmanová J, Skalníková M, Kozubek M, Kozubek S. 2005. Nuclear levels and patterns of histone H3 modification and HP1 proteins after inhibition of histone deacetylases. J Cell Sci 18:5035–5046.

Bártová E, Harničarová A, Krejčí J, Strašák L, Kozubek S. 2008. Single-cell c-myc gene expression in relationship to nuclear domains. Chromosome Res 16:325–343.

Bolzer A, Kreth G, Solovei I, Koehler D, Saracoglu K, Fauth C, Müller S, Eils R, Cremer C, Speicher MR, Cremer T. 2005. Three-dimensional maps of all chromosomes in human male fibroblast nuclei and prometaphase rosettes. PLoS Biol 3(5):e157.

Boveri T. 1909. Die Blastomerenkerne von *Ascaris megalocephala* und die Theorie der Chromosomenindividualität. Arch Zellforsch 3:181–268.

Caron H, van Schaik B, van der Mee M, Baas F, Riggins G, van Sluis P, Hermus MC, van Asperen R, Boon K, Voûte PA, Heisterkamp S, van Kampen A, Versteeg R. 2001. The human transcriptome map: Clustering of highly expressed genes in chromosomal domains. Science 291:1289–1292.

Chaly N, Munro S. 1996. Centromeres reposition to the nuclear periphery during L6E9 myogenesis in vitro. Exp Cell Res 223:274–278.

Chubb JR, Boyle S, Perry P, Bickmore WA. 2002. Chromatin motion is constrained by association with nuclear compartments in human cells. Curr Biol 12:439–445.

Cremer T, Cremer C. 2001. Chromosome territories, nuclear architecture and gene regulation in mammalian cells. Nat Rev Genet 2:292–301.

Cremer T, Cremer M. 2011. Chromosome territories. The nucleus. Cold Spring Harbor Laboratory Press. pp 93–114.

Cremer T, Cremer C, Baumann H, Baumann H, Hens L, Kirsch-Volders M. 1982. Rabl's model of the interphase chromosome arrangement tested in Chinese hamster cells by premature chromosome condensation and laser-UV-microbeam experiments. Hum Genet 60:46–56.

Croft JA, Bridger JM, Boyle S, Perry P, Teague P, Bickmore WA. 1999. Differences in the localization and morphology of chromosomes in the human nucleus. J Cell Biol 145:1119–1131.

Cvačková Z, Mašata M, Staněk D, Fidlerová H, Raška I. 2009. Chromatin position in human HepG2 cells: Although being non-random, significantly changed in daughter cells. J Struct Biol 165:107–117.

Dundr M. 2012. Nuclear bodies: Multifunctional companions of the genome. Curr Opin Cell Biol 24:1–8.

Essers J, van Cappellen WA, Theil AF, van Drunen E, Jaspers NG, Hoeijmakers JH, Wyman C, Vermeulen W, Kanaar R. 2005. Dynamics of relative chromosome position during the cell cycle. Mol Biol Cell 16:769–775.

Fernandez-Capetillo O, Lee A, Nussenzweig M, Nussenzweig A. 2004. H2AX: The histone guardian of the genome. DNA Repair 3:959–967.

Francastel C, Schubeler D, Martin DI, Groudine M. 2000. Nuclear compartmentalization and gene activity. Nat Rev Mol Cell Biol 1:137–143.

Galiová G, Bártová E, Raška I, Krejčí J, Kozubek S. 2008. Chromatin changes induced by lamin A/C deficiency and the histone deacetylase inhibitor trichostatin A. Eur J Cell Biol 87:291–303.

Gerlich D, Beaudouin J, Kalbfuss BG. 2003. Global chromosome positions are transmitted through mitosis in mammalian cells. Cell 112:751–764.

Gierman HJ, Indemans MH, Koster J, Goetze S, Seppen J, Geerts D, van Driel R, Versteeg R. 2007. Domain-wide regulation of gene expression in the human genome. Genome Res 17(9):1286–1295.

Goetze S, Mateos-Langerak J, Gierman HJ, de Leeuw W, Giromus O, Indemans MH, Koster J, Ondrej V, Versteeg R, van Driel R. 2007. The 3D structure of human interphase chromosomes is related to the transcriptome map. Mol Cell Biol 27:4475–4487.

Grewal S, Jia S. 2007. Heterochromatin revisited. Nature Reviews Genetics 8:35–46.

Gurskaya NG, Verkhusha VV, Shcheglov AS, Staroverov DB, Chepurnykh TV, Fradkov AF, Lukyanov S, Lukyanov KA. 2006. Engineering of a monomeric green-to-red photoactivatable fluorescent protein induced by blue light. Nat Biotechnol 24:461–465.

Haralick RM. 1979. Statistical and structural approaches to texture. Proc IEEE 67:786–804.

Harničarová A, Kozubek S, Pacherník J, Krejčí J, Bártová E. 2006. Distinct nuclear arrangement of active and inactive c-myc genes in control and differentiated colon carcinoma cells. Exp Cell Res 312:4019–4035.

Hawkins N, Garriga G. 1998. Asymmetric cell division: From A to Z. Genes Dev 12:3625–3638.

Hofer M, Dušek L, Hoferová Z, Stixová L, Pospíšil M. 2011. Expression of mRNA for adenosine A(1), A(2a), A(2b), and A(3) receptors in HL-60 cells: Dependence on cell cycle phases. Physiol Res 60:913–920.

Katan-Khaykovich Y, Struhl K. 2011. Splitting of H3-H4 tetramers at transcriptionally active genes undergoing dynamic histone exchange. Proc Natl Acad Sci USA 108:1296–1301.

Kozubek S, Lukášová E, Rýznar L, Kozubek M, Lišková A, Govorun RD, Krasavin EA, Horneck G. 1997. Distribution of ABL and BCR genes in cell nuclei of normal and irradiated lymphocytes. Blood 89:4537–4545.

Kozubek M, Kozubek S, Lukášová E, Marečková A, Bártová E, Skalníková M, Jergová A. 1999a. High-resolution cytometry of FISH dots in interphase cell nuclei. Cytometry 36:279–293.

Kozubek S, Lukášová E, Marečková A, Skalníková M, Kozubek M, Bártová E, Kroha V, Krahulcová E, Šlotová J. 1999b. The topological organization of chromosomes 9 and 22 in cell nuclei has a determinative role in the induction of t(9,22) translocations and in the pathogenesis of t(9,22) leukemias. Chromosoma 108:426–435.

Kozubek M, Kozubek S, Lukášová E, Bártová E, Skalníková M, Matula P, Jirsová P, Cafourková A, Koutná I. 2001. Combined confocal and wide-field high-resolution cytometry of fluorescent in situ hybridization-stained cells. Cytometry 45:1–12.

Kozubek S, Lukášová E, Jirsová P, Koutná I, Kozubek M, Gaňová A, Bártová E, Falk M, Paseková R. 2002. 3D Structure of the human genome: Order in randomness. Chromosoma 111:321–331.

Kurz A, Lampel S, Nickolenko JE, Bradl J, Benner A, Zirbel RM, Cremer T, Lichter P. 1996. Active and inactive genes localize preferentially in the periphery of chromosome territories. J Cell Biol 135:1195–1205.

Lanctôt C, Cheutin T, Cremer M, Cavalli G, Cremer T. 2007. Dynamic genome architecture in the nuclear space: Regulation of gene expression in three dimensions. Nat Rev Genet 8:104–115.

Lieberman-Aiden E, van Berkum NL, Williams L, Imakaev M, Ragoczy T, Telling A, Amit I, Lajoie BR, Sabo PJ, Dorschner MO, Sandstrom R, Bernstein B, Bender MA, Groudine M, Gnirke A, Stamatoyannopoulos J, Mirny LA, Lander ES, Dekker J. 2009. Comprehensive mapping of long-range interactions reveals folding principles of the human genome. Science 326:289–293.

Martin FL, Cole KJ, Orme MH, Grover PL, Phillips DH, Venitt S. 1999. The DNA repair inhibitors hydroxyurea and cytosine arabinoside enhance the sensitivity of the alkaline single-cell gel electrophoresis ('comet') assay in metabolically-competent MCL-5 cells. Mutat Res 445:21–43.

Meaburn KJ, Gudla PR, Khan S, Lockett SJ, Misteli T. 2009. Disease-specific gene repositioning in breast cancer. J Cell Biol 187:801–812.

Müller I, Boyle S, Singer RH, Bickmore WA, Chubb JR. 2010. Stable morphology, but dynamic internal reorganisation, of interphase human chromosomes in living cells. PLoS ONE 5(7):e11560.

Nagy Z, Soutoglou E. 2009. DNA repair: Easy to visualize, difficult to elucidate. Trends Cell Biol 19:617–629.

Nikiforova MN, Stringer JR, Blough R, Medvedovic M, Fagin JA, Nikiforov YE. 2000. Proximity of chromosomal loci that participate in radiation-induced rearrangements in human cells. Science 290:138–141.

Ojala T, Pietikäinen M, Harwood D. 1996. A comparative study of texture measures with classification based on feature distributions. Pattern Recognit 29:51–59.

Parada L, Misteli T. 2002. Chromosome positioning in the interphase nucleus. Trends Cell Biol 12:425–432.

Parada LA, McQueen PG, Munson PJ, Misteli T. 2002. Conservation of relative chromosome positioning in normal and cancer cells. Curr Biol 12:1692–1697.

Rabl C. 1885. Űber Zelltheilung. Morpholog Jahrbuch 10:214–330.

Rogakou EP, Pilch DR, Orr AH, Ivanova VS, Bonner WM. 1998. DNA double-stranded breaks induce histone H2AX phosphorylation on serine 139. J Biol Chem 273(10):5858–5868.

Simonis M, Klous P, Splinter E, Moshkin Y, Willemsen R, de Wit E, van Steensel B, de Laat W. 2006. Nuclear organization of active and inactive chromatin domains uncovered by chromosome conformation capture-on-chip (4C). Nat Genet 38:1348–1354.

Soille P. 2004. Morphological image analysis: Principles and applications, 2nd edition. Berlin: Springer-Verlag.

Spiegel MR. 1992. Correlation theory. Chapter 14 in theory and problems of probability and statistics, 2nd edition. New York: McGraw-Hill. pp 294–323.

Sporbert A, Domaing P, Leonhardt H, Cardoso MC. 2005. PCNA acts as a stationary loading platform for transiently interacting Okazaki fragment maturation proteins. Nucleic Acids Res 33:3521–3528.

Stixová L, Bártová E, Matula P, Daněk O, Legartová S, Kozubek S. 2011. Heterogeneity in the kinetics of nuclear proteins and trajectories of substructures associated with heterochromatin. Epigenet Chromatin 4:5.

Strašák L, Bártová E, Harničarová A, Galiová G, Krejčí J, Kozubek S. 2009. H3K9 acetylation and radial chromatin positioning. J Cell Physiol 220:91–101.

Strickfaden H, Zunhammer A, van Koningsbruggen S, Köhler D, Cremer T. 2010. 4D chromatin dynamics in cycling cells: Theodor Boveri's hypotheses revisited. Nucleus 1:284–297.

Šustáčková G, Kozubek S, Stixová L, Legartová S, Matula P, Orlova D, Bártová E. 2012a. Acetylation-dependent nuclear arrangement and recruitment of BMI1 protein to UV-damaged chromatin. J Cell Physiol 227:1838–1850.

Šustáčková G, Legartová S, Kozubek S, Stixová L, Pacherník J, Bártová E. 2012b. Differentiation-independent fluctuation of pluripotency-related transcription factors and other epigenetic markers in embryonic stem cell colonies. Stem Cells Dev 21:710–720.

Takizawa T, Gudla PR, Guo L, Lockett S, Misteli T. 2008. Allele-specific nuclear positioning of the monoallelically expressed astrocyte marker GFAP. Genes Dev 22:489–498.

Taslerová R, Kozubek S, Lukášová E, Jirsová P, Bártová E, Kozubek M. 2003. Arrangement of chromosome 11 and 22 territories, EWSR1 and FLI1 genes, and other genetic elements of these chromosomes in human lymphocytes and Ewing sarcoma cells. Hum Genet 112:143–155.

Thomson I, Gilchrist S, Bickmore WA, Chubb JR. 2004. The radial positioning of chromatin is not transmitted through mitosis but is established de novo in early G1. Curr Biol 14:166–172.

Versteeg R, van Schaik BD, van Batenburg MF, Roos M, Monajemi R, Caron H, Bussemaker HJ, van Kampen AH. 2003. The human transcriptome map reveals extremes in gene density, intron length, GC content, and repeat pattern for domains of highly and weakly expressed genes. Genome Res 13:1998–2004.

Walter J, Schermelleh L, Cremer M, Tashiro S, Cremer T. 2003. Chromosome order in HeLa cells changes during mitosis and early G1, but is stably maintained during subsequent interphase stages. J Cell Biol 160:685–697.

Wiblin AE, Cui W, Clark AJ, Bickmore WA. 2005. Distinctive nuclear organisation of centromeres and regions involved in pluripotency in human embryonic stem cells. J Cell Sci 118:3861–3868.

Wildanger D, Rittweger E, Kastrup L, Hell SW. 2008. STED microscopy with a supercontinuum laser source. Opt Express 16(13):9614–9621.

Williams RR, Broad S, Sheer D, Ragoussis J. 2002. Subchromosomal positioning of the epidermal differentiation complex (EDC) in keratinocyte and lymphoblast interphase nuclei. Exp Cell Res 272:163–175.

Zink D, Cremer T. 1998. Cell nucleus: Chromosome dynamics in nuclei of living cells. Curr Biol 8:R321–R324.

Zolghadr K, Mortusewicz O, Rothbauer U, Kleinhans R, Goehler H, Wanker EE, Cardoso MC, Leonhardt H. 2008. A fluorescent two-hybrid assay for direct visualization of protein interactions in living cells. Mol Cell Proteomics 7:2279–2287.